Ab initio total-energy calculations for iron-acceptor pairs in silicon

H. Overhof and H. Weihrich
Fachbereich Physik, Universität-GH Paderborn, D-33095 Paderborn, Federal Republic of Germany
(Received 13 November 1996)

We present *ab initio* total-energy calculations for trigonal and orthorhombic iron-acceptor pairs in silicon. The total-energy calculations have been performed in the general framework of the density-functional theory treating many-particle effects in the local spin-density approximation. We use a Green's-function approach based on the linear muffin-tin orbitals theory using the atomic-sphere approximation (which unfortunately prohibits the inclusion of any lattice-relaxation effects). Our total-energy calculations lead to a model for the electronic structure of both orthorhombic and trigonal pairs that is dominated by ionic binding of the interstitial iron to the acceptor on a substitutional site and does not predict a significant covalent binding of the pair. This is in contrast to the case of Fe_i-Au_{Si} and Fe_i-Ag_{Si} pairs for which there is a strong covalent pair binding for any position of the Fermi energy. In agreement with the ionic-binding model, we do not find pairing in *n*-type material for any iron-acceptor pairs. We find, however, that in *n*-type material there is moderately strong pairing of iron with shallow donors (P_{Si}^{+} for example), again in agreement with an ionic model for the pair formation. [S0163-1829(97)03016-6]

INTRODUCTION

Iron is a ubiquitous interstitial impurity in silicon (for a recent comprehensive review see, e.g., Ref. 1), which, due to its rather high mobility combined with a rather low solubility, has a strong tendency to form pairs and also larger aggregates with other point defects present in the material. Pair formation of interstitial iron with shallow acceptors is a delicate process: pairs do not form at elevated temperatures in *p*-type material. However, after quenching at room temperature the pairs form within hours[1] and easily dissociate again at elevated temperatures,[2] under illumination with white light,[2] or under electron injection.[3] In *n*-type samples that are partly compensated by boron, iron-boron pairs have not been observed.[1] Instead, in *n*-type silicon the formation of an iron-phosphorus complex has been observed indirectly[4] via the disappearance of the electron paramagnetic resonance (EPR) of the neutral interstitial Fe_i^0 signal.

The greatest interest in the iron-acceptor pair formation arises from the observed metastability of the iron-acceptor pairs.[5,6] EPR investigations have shown that all pairs can be observed both with trigonal and with orthorhombic symmetry and also in several charge states.[7–15] While in the earlier papers[5,6] it was assumed that the pair binding is essentially due to the ionic binding between the negatively charged acceptor and the positively charged iron, this interpretation has been questioned on the basis of *ab initio* calculations by Assali and Leite,[16–19] who find a strong covalent mixing of the iron-derived states with the acceptor states. These authors, however, have not examined the pair binding energies as a function of the Fermi level position and therefore it is not clear whether their covalent model can explain that the pair stability depends on the position of the Fermi energy.

In this paper we calculate the electronic structure and in particular the pair formation energy of pairs consisting of interstitial iron with substitutional B, Al, Ga, and In acceptors both in trigonal and in orthorhombic configurations as a function of the Fermi-level position. In Sec. I we briefly sketch the method used for the total-energy computation. We then describe the pair formation energies and compare electron removal energies with the respective experimental data in Sec. II. The results are discussed in Sec. III in comparison with the results of Assali and Leite.[16–19]

An extremely close check of our theoretical results would be provided by a detailed comparison of our calculated hyperfine interactions with the experimental results of EPR and electron-nuclear double resonance. This is planned to be presented in a forthcoming paper (Ref. 20) because the presentation of the computational method used (and of the many results) calls for a separate paper.

I. TOTAL-ENERGY CALCULATIONS

A. Theoretical method

We have performed *ab initio* total-energy calculations using the density-functional theory[21,22] in the local spin-density approximation[23–25] to determine the electronic ground-state properties of the iron-acceptor pairs in silicon. The computational scheme has been discussed in detail in a theoretical paper[26] as well as in several applications[27,28] and very recently the application to isolated interstitial iron was presented.[29] We therefore restrict the presentation of the theoretical method to the few points that are specific to the applications to pairs.

We solve the problem of a deep impurity in a silicon crystal using a Green's-function technique and solving a Dyson equation

$$G(\vec{r},\vec{r}',z)=G^0(\vec{r},\vec{r}',z)+\int G^0(\vec{r},\vec{r}'',z)\triangle V(\vec{r}'') \times G(\vec{r}'',\vec{r}',z)d^3\vec{r}'', \quad (1)$$

where $\triangle V=V-V^0$ is the difference between the one-particle potentials of the crystal containing the impurity and that of the unperturbed crystal. We first carry out a band-

structure calculation using the linear muffin-tin orbital method in the atomic-sphere approximation (ASA) in order to determine the Green's function G^0 of the unperturbed crystal. Since for deep impurities the difference of the potentials $\triangle V$ has large values in a small region around the impurity only, we divide the crystal into a ''perturbed region'' containing the atomic spheres of the impurity atom, of a few neighboring silicon host atoms and of space-filling interstitial spheres, and into the ''unperturbed'' crystal outside this region. Our perturbed region consists of 29 atomic spheres that contain silicon atoms, of 27 empty spheres, and of the two atomic spheres centered around the two impurity atoms. Within the perturbed region Dyson's equation is solved self-consistently; outside this region G is approximated by G^0.

The total energy of the crystal containing an isolated point defect or a pair defect is calculated ignoring lattice relaxations.[26–28] We directly calculate the change in total energy introduced by the defects.[26] To this quantity we add the energy of the long-range Coulomb part of $n\times 0.1$ eV, where n indicates the charge state of the impurity.[27,30] In order to compare total energies for different charge states of a defect we discuss the n-times charged defect $D^{(n)}$ plus n electrons or holes that are transferred to the Fermi level. Thus the total energy becomes a function of the Fermi level E_F,

$$E_{\rm tot}(D^{(n)},E_F)=E^b_{\rm tot}(D^{(n)})+nE_F, \tag{2}$$

where $E^b_{\rm tot}$ is the energy of the defect for a Fermi level at the valence-band edge. With these total energies we calculate the electron removal energies, which is that position of the Fermi level for which the total energies of two charge states coincide.

The pair binding energy is calculated as the difference between the sum of the total energies of the two constituents and the total energy of the pair

$$E_{\rm bind}((\mathrm{Fe}_i-\mathcal{A}_{\rm Si})^{(n)},E_F)=E_{\rm tot}(\mathrm{Fe}_i^{(n+1)},E_F)+E_{\rm tot}(\mathcal{A}_{\rm Si}^{(-)},E_F) -E_{\rm tot}((\mathrm{Fe}_i-\mathcal{A}_{\rm Si})^{(n)},E_F). \tag{3}$$

Note that in this definition $E_{\rm bind}$ is positive if the constituents attract each other. The charge states both of the pair and of the interstitial iron in Eq. 3 are chosen to minimize the respective value of $E_{\rm tot}$ for a given position of E_F. The charge state of the pair therefore may differ from the sum of the charges attributed to the constituents. The pair binding energy depends on the position of the Fermi energy E_F because the electron removal energies of the pair will not coincide with those of the constituents.

II. RESULTS

A. Trigonal pairs

For the trigonal pairs we have studied several configurations where the iron atom was situated on one of the tetrahedral interstitial sites and the acceptor was on one of the regular lattice sites. Figure 1 gives a sketch of the atomic arrangements in the (110) plane for the trigonal pair configurations studied. Since in all cases studied the pair binding energy $E_{\rm bind}((\mathrm{Fe}_i-\mathcal{A}_{\rm Si})^{(n)},E_F)$ for the pair A was much larger than for the pairs B-D we shall concentrate mainly on pair A.

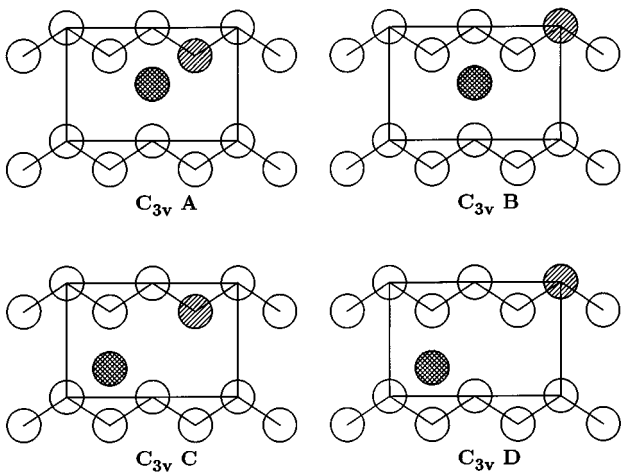

FIG. 1. Sketch of the four atomic configurations in a (110) plane for the trigonal pairs. The iron atom is represented by a cross-hatched sphere, the acceptor atom is given by a hatched sphere, while the silicon atoms are left blank.

We display in Fig. 2(a) a contour plot of the magnetization density for the neutral trigonal $(\mathrm{Fe}_i\text{-}\mathrm{Al}_{\rm Si})^0$ pair A in the (110) plane and in Fig. 2(b) we show a contour plot of the induced particle density. These contour plots are very similar for all trigonal pairs if the 3d electrons of Ga (and the 4d electrons of In) are ignored. It is evident from Fig. 2(b) that the electron density of the acceptor $\mathrm{Al}^-_{\rm Si}$ is smaller than that of the Si atom that it substitutes. However, if compared with the corresponding figure for isolated Fe_i^+ (see Ref. 29, Fig. 6) this obviously is the only major change of the induced particle density distribution upon pair formation. The respective magnetization density distribution for the pair also resembles that of isolated Fe_i^+ if for the latter a trigonal symmetry is assumed. Note that again the magnetization density

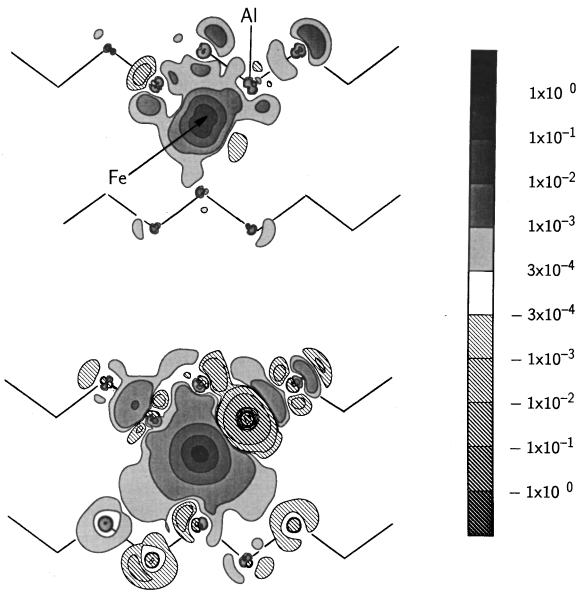

FIG. 2. Contour plot of (a) the magnetization density and (b) the induced particle density (b) in the (110) plane for the neutral trigonal $(\mathrm{Fe}_i\text{-}\mathrm{Al}_{\rm Si})^0$ pair A. The positions of the nuclei are indicated by arrows in (a).

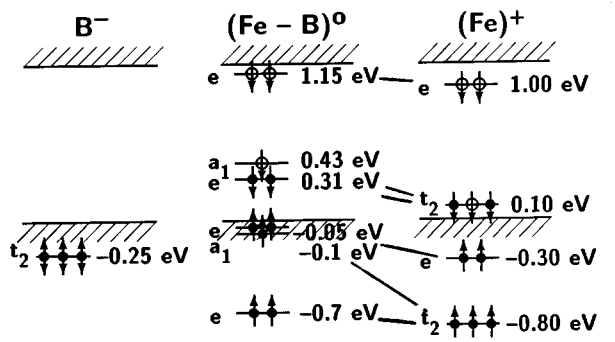

FIG. 3. Energy-level diagram for the formation of the neutral trigonal FeB pair. The t_2 states of isolated B_{Si}^- are shown on the left-hand side and the energy levels of the antibonding states of Fe_i^+ are shown on the right-hand side. For the neutral pair also only the antibonding states are shown. Full circles mark occupied states.

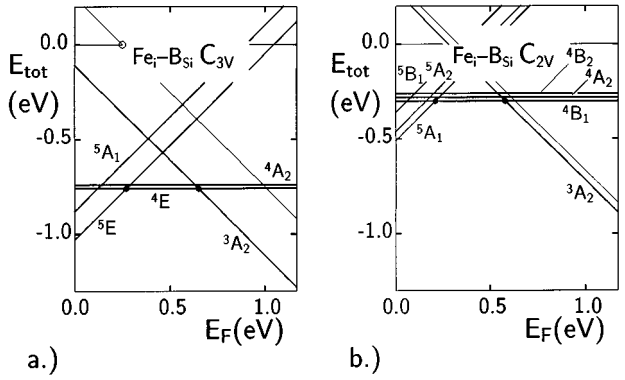

FIG. 4. Total energies $E_{tot}((Fe_i\text{-}B_{Si})^{(n)},E_F)$ (full lines) for (a) the trigonal pair A and (b) the orthorhombic pair in different electronic states and charge states as a function of the Fermi energy. Energies for the positively charged, neutral, and negatively charged states have the slopes $+1$, 0, and -1, respectively. Full circles mark electron removal energies of the pairs. Thin lines give the total energies of dissociated pairs. The zero of the energy scale is chosen to coincide with the energy of the neutral dissociated pair.

is significantly more localized than the induced particle density, which has a pronounced oscillatory character.

The structure of the induced density of states (DOS) of the pairs can easily be interpreted with the help of the bonding and antibonding states of the isolated Fe_i.[29] The resonant states that for isolated Fe_i could be clearly identified as bonding states of the iron with the silicon ligands are present for the pairs as well. Due to the lower symmetry of the pairs the resonances are much broader and therefore not easily detected in a DOS distribution plot. We therefore leave out these states in Fig. 3. Instead we show as a representative example for all pairs the antibonding resonant states and localized gap states for the neutral trigonal $(Fe_i\text{-}B_{Si})^0$ pair in comparison with the states of the constituents B_{Si}^- and Fe_i^+, respectively. The acceptor states that for the isolated acceptors transform according to the t_2 irreducible representation form a sharp resonance just below the valence-band edge. These states, however, must not be regarded as additional states because these states act as a replacement for the t_2 states of the silicon atom that has been substituted by the acceptor. The states of the Si atom that has been substituted show up as a broad negative resonance in the induced DOS distribution. These broad negative resonances overlap in part with the broad bonding resonances originating from the iron and are also not included in the figure.

The main influence of the acceptor in the pair formation comes from its negative charge, which also gives rise to the trigonal crystal field. This field splits the states that have transformed according to the t_2 irreducible representation of the cubic group T_d into states that transform according to the a_1 and e irreducible representations of the group C_{3v}.

It is evident from Fig. 3 that the negative charge of the acceptor does not affect the different states in the same way. In particular the shift of the $a_1^\uparrow$ level is with 0.7 eV quite large, while the corresponding $e^\uparrow$ state is hardly affected. Upon pair formation there must therefore be a significant redistribution of the particle density within the different antibonding localized states and resonances. There is also a significant shift of the bonding states not included in Fig. 3.

For the gap states the trigonal field essentially leads to a minor splitting of the $t_2^\downarrow$ states into an $a_1^\downarrow$ and an $e^\downarrow$ state only. There is little admixture of the $t_2^\downarrow$-derived states to the upper $e^\downarrow$ state. This can be seen directly if one compares the 0.08-eV a_1-e splitting with the ten times larger t_2-e splitting that originates from the cubic field. The upper $e^\downarrow$ states can therefore be considered to a good approximation as a state that transforms according to the e irreducible representation of the group T_d.

In Fig. 4(a) we show the total energies of the trigonal $Fe_i\text{-}B_{Si}$ pairs in the different charge states and for different ground state configurations as a function of the Fermi energy. For all charge states of the pairs we find the high-spin state as the ground state. We also observe that for the positively charged and the neutral pair there are two different high-spin states that are nearly degenerate. This point will be of major importance when calculating hyperfine interactions (see Ref. 20).

The sum of all changes of the densities that accompany the energetic splittings and shifts documented in Fig. 3 are extremely small. Tables I and II demonstrate that the integrals of the spin densities contained in the different ASA spheres, $n^\uparrow$, $n^\downarrow$, n^{tot}, and $m_0=n^\uparrow-n^\downarrow$ for the neutral pairs, virtually coincide with the sums of the respective values for the isolated acceptor and isolated Fe_i^+. For the pairs in the negative-charge state, in a similar way $n^\uparrow$, $n^\downarrow$, n^{tot}, and m_0 for the iron, the acceptor, and the Si(1,1,1) ASA spheres of the iron-acceptor pairs can be approximated quite nicely by summing up the corresponding values for the isolated acceptor and the isolated neutral Fe_i^0 deep defects. This is understood if we recall that the substitution of a silicon atom by the acceptor is not accompanied by the introduction of additional states. Since in addition the acceptor is essentially diamagnetic, the magnetization of the iron ASA spheres of the pairs also does not deviate significantly from that of the isolated interstitial iron.

The values of n^{tot} for the acceptors require several comments. Since the boron $2p$ states are very localized the induced density in this ASA sphere is nearly zero, i.e., the particle density is nearly equal to the particle density contained in a regular silicon ASA sphere. In contrast, the Al $3p$ states are more extended and therefore in the Al ASA

TABLE I. Calculated induced spin density integrated within different ASA spheres for isolated point defects.

Integrated density	Fe_i		$\mathcal{A}_{Si}^-$			
	Fe_i^+	Fe_i^-	B_{Si}^-	Al_{Si}^-	Ga_{Si}^-	In_{Si}^-
$n_{ind}^{\uparrow,defect}(0,0,0)$	4.6699	4.4588	−0.0793	−0.4864	4.7235	4.4500
$n_{ind}^{\downarrow,defect}(0,0,0)$	2.3109	2.5788	−0.0793	−0.4864	4.7235	4.4500
$n_{ind}^{tot,defect}(0,0,0)$	6.9808	7.0376	−0.1586	−0.9828	9.4470	8.8901
$m_0^{defect}(0,0,0)$	2.3590	1.8800				
$n_{ind}^{\uparrow,Si}(\overline{1,1,1})$	0.0829	0.0656	−0.0003	0.0055	−0.0076	0.0163
$n_{ind}^{\downarrow,Si}(\overline{1,1,1})$	0.0391	0.0604	−0.0003	0.0055	−0.0076	0.0163
$n_{ind}^{tot,Si}(\overline{1,1,1})$	0.1220	0.1260	−0.0006	0.0110	−0.0152	0.0336

sphere there is virtually one electron missing (70% of which is spread over the adjacent ASA spheres). The Ga and In ASA spheres in addition contain the ten $3d$ (Ga) and $4d$ (In) electrons. While the Ga $3d$ states are well localized within the Ga ASA sphere, the larger size of the In $4d$ states prohibits a complete accommodation of these states within the In ASA sphere.

B. Orthorhombic pairs

We have studied orthorhombic pairs where the interstitial iron and the substitutional acceptor are separated by one-half of a lattice constant. Alternative orthorhombic pairs (with both constituents accommodated on tetrahedral interstitial and substitutional sites, respectively) have such a large separation of the two constituents that within computational error no interaction was observed.

We show the energies of the antibonding states of the neutral orthorhombic iron-acceptor pairs in Fig. 5 in comparison with the corresponding states of Fe_i^+. As in the case of the trigonal pairs, we leave out the rather broad bonding resonances. The orthorhombic field splits all states that transform according to the t_2 irreducible representation of the group T_d into states that transform according to a_1, b_1, and b_2, respectively. The former e states are split into a_1 and a_2. These will be denoted by $\hat{a}_1$ and $\hat{a}_2$, respectively, because our calculated electron density distributions show that there is virtually no mixing between the a_1 states originating from the former t_2 states and the $\hat{a}_2$ states that originate from the former e states.

The ground state for all charge states of the orthorhombic pairs trivially must be an orbital singlet because all the irreducible single-group representations of the group C_{2v} are one dimensional. We also obtain high-spin states as ground states as in the case of isolated Fe_i^0 and Fe_i^+. As in the case of the trigonal pairs, there are several different high-spin states for the positively charged and for the neutral charged pairs as shown in Fig. 4(b). The differences between the total energies for the different states of the positively charged and the neutral pairs are again small and comparable to the spin-orbit interaction. This latter interaction must therefore be taken into account when calculating the hyperfine interactions. For the negatively charged pairs the ground state is an orbital singlet without a localized excited state. For this charge state the spin-orbit interaction will therefore be less important.

The magnetization densities and induced particle densities for the neutral orthorhombic FeAl pair are shown in Fig. 6. As was the case for the trigonal pairs, the contour plots are hardly different from a proper symmetric superposition of the contour plots of the isolated point defect that make up the

TABLE II. Calculated induced spin density integrated within different ASA spheres for trigonal iron-acceptor pairs.

Integrated density	Trigonal $(Fe_i\text{-}\mathcal{A}_{Si})^0$ pairs				Trigonal $(Fe_i\text{-}\mathcal{A}_{Si})^-$ pairs			
	$(Fe_i\text{-}B_{Si})^0$	$(Fe_i\text{-}Al_{Si})^0$	$(Fe_i\text{-}Ga_{Si})^0$	$(Fe_i\text{-}In_{Si})^0$	$(Fe_i\text{-}B_{Si})^-$	$(Fe_i\text{-}Al_{Si})^-$	$(Fe_i\text{-}Ga_{Si})^-$	$(Fe_i\text{-}In_{Si})^-$
$n_{ind}^{\uparrow,(Fe_i)}$	4.7544	4.6830	4.6091	4.6390	4.4698	4.4566	4.4343	4.4791
$n_{ind}^{\downarrow,(Fe_i)}$	2.1163	2.2983	2.3174	2.3748	2.4597	2.5747	2.5425	2.5752
$n_{ind}^{tot,(Fe_i)}$	6.8707	6.9814	6.9266	7.0138	6.9295	7.0313	6.9769	7.0543
$m_0^{(Fe_i)}$	2.5381	2.3847	2.2917	2.2642	2.0101	1.8819	1.9918	1.9039
$n_{ind}^{\uparrow,(\mathcal{A}_{Si})}$	+0.0100	−0.3981	4.8263	4.5539	0.0020	−0.4104	4.7966	4.5308
$n_{ind}^{\downarrow,(\mathcal{A}_{Si})}$	−0.0457	−0.4491	4.7598	4.5067	−0.0435	−0.4341	4.7687	4.5058
$n_{ind}^{tot,(\mathcal{A}_{Si})}$	−0.0357	−0.8472	9.5861	9.0606	−0.0414	−0.8445	9.5654	9.0365
$n_{ind}^{\uparrow,Si(2,2,2)}$	0.0816	0.0718	0.0707	0.0652	0.0697	0.0594	0.0590	0.0542
$n_{ind}^{\downarrow,Si(2,2,2)}$	0.0666	0.0538	0.0577	0.0636	0.0684	0.0577	0.0613	0.0559
$n_{ind}^{tot,Si(2,2,2)}$	0.1482	0.1256	0.1284	0.1188	0.1381	0.1171	0.1203	0.1101

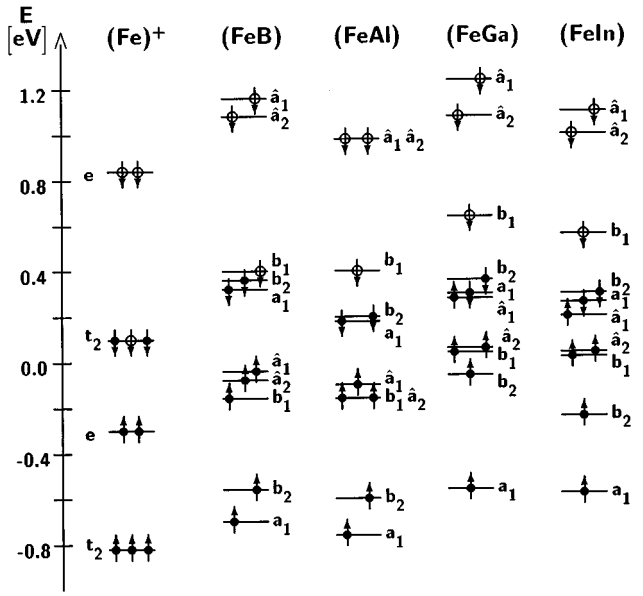

FIG. 5. Energy-level diagram for the antibonding states of the neutral orthorhombic Fe-$\mathcal{A}$ pairs. The energy levels of the antibonding states for isolated Fe_i^+ are shown on the left-hand side for comparison. The states that originate from the former e states of Fe_i^+ are denoted by $\hat{a}_1$ and $\hat{a}_2$, respectively.

pair. This is also true for the densities projected into the ASA spheres. In an orthorhombic symmetry the more delocalized nature of the induced particle density as compared with the magnetization density appears to be even more pronounced than in the trigonal pair.

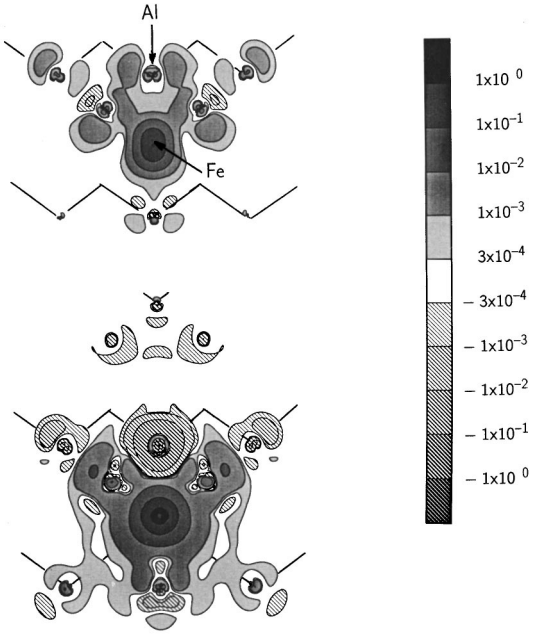

FIG. 6. Contour plot of (a) the magnetization density and (b) the induced particle density in the (110) plane for the neutral orthorhombic $(Fe_i\text{-}Al_{Si})^0$ pair. The positions of the nuclei are indicated by arrows in (a).

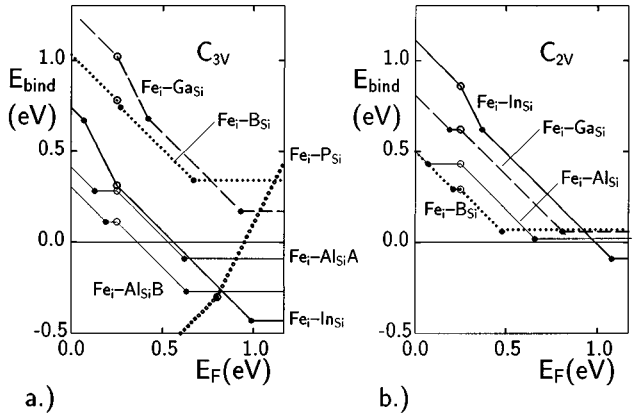

FIG. 7. Pair formation energies $E_{\mathrm{bind}}((Fe_i\text{-}\mathcal{A}_{Si})^{(n)},E_F)$ for (a) trigonal $Fe_i\text{-}\mathcal{A}_{Si}$ and (b) orthorhombic pairs as a function of the Fermi energy. Full circles mark electron removal energies of the pairs. For trigonal $Fe_i\text{-}\mathcal{A}_{Si}$ results for the configurations A and B (see Fig. 1) are given. Results for a trigonal $Fe_i\text{-}P_{Si}$ pair are also shown in (a).

III. DISCUSSION

In Fig. 7 we compare the calculated pair formation energies E_{bind} for (a) the trigonal pairs and (b) the orthorhombic pairs as a function of the Fermi energy E_F. We see that for most acceptors and both pair geometries the pairs do not bind unless the Fermi energy is in the lower half of the gap. Exceptions are the trigonal $Fe_i\text{-}B_{Si}$ and $Fe_i\text{-}Ga_{Si}$ pairs. But for these pairs also the pair binding energy for n-type crystals would be rather small. Clearly all pairs are unstable at elevated temperatures when the Fermi energy moves into the center of the gap. All these results are in general qualitative agreement with the experimental observations.[1]

From an inspection of Table I we see that the B_{Si}^- and Ga_{Si}^- acceptors are rather small, i.e., the total valence electron density is contained nearly completely within the ASA sphere. For these acceptors the close trigonal pair is energetically favorable in particular, whereas for the large In_{Si}^- acceptor the more distant orthorhombic pair configuration has the larger binding energy.

For $Fe_i\text{-}B_{Si}$ and for $Fe_i\text{-}Al_{Si}$ we can compare quantitatively the validity of our pair binding energies E_{bind} with experimental data. The experimental value for $Fe_i\text{-}B_{Si}$, 0.65 ± 0.02 eV,[33] compares well with our calculated value of 0.78 eV. For $Fe_i\text{-}Al_{Si}$ the corresponding values are 0.47 (Ref. 5) and 0.28 eV, respectively. Kimerling *et al.*[6,33] have determined the relative populations for the trigonal versus orthorhombic states of the pairs in their negative- and positive-charge states. A comparison of the total-energy differences obtained from this ratio with calculated total-energy differences is given in Table III. We see that qualitatively the energy differences for the $Fe_i\text{-}B_{Si}$ and for the $Fe_i\text{-}Al_{Si}$ pairs compare well with the experimental data, but for the $Fe_i\text{-}In_{Si}$ and even more for the $Fe_i\text{-}Ga_{Si}$ the discrepancies are greater than the experimental values. This is not entirely unexpected. The introduction of the Ga and In acceptors is a major perturbation of the Si lattice because of the filled d shells, which hybridize with the valence-band states. Although these states are nearly corelike, this hybridization will lead to large changes in total energy and any slight distortion

TABLE III. Comparison of the experimentally determined and calculated difference of the total energies for trigonal and orthorhombic Fe-$\mathcal{A}$ pairs (in eV).

	$(Fe_i\text{-}\mathcal{A}_{Si})^+$		$(Fe_i\text{-}\mathcal{A}_{Si})^0$	
Pair	Expt.[a]	This work	Expt.[a]	This work
FeB	>0.1	0.34	>0.1	0.26
FeAl	0.02	0.08	0.09	0.16
FeGa	0.04	0.44	0.14	0.23
FeIn	-0.13	0.37	0.01	-0.08

[a]Reference 33.

of these states upon pair formation will introduce errors that can easily amount to a few tenths of an eV. A comparison with the much simpler electrostatic and polarization models[33,34] shows that these models predict the pair binding energies in a much more reliable way.

If we compare the calculated electron removal energies (Table IV) with experimentally determined values we find general agreement. The trends observed experimentally, however, are not reproduced satisfactorily in our calculations. This may be due to the fact that the ASA and the neglect of lattice relaxation introduce errors that depend sensitively on the size of the acceptor ion.

Recently, Nakashima *et al.*[32] have determined the electron removal energies for several different configurations of the Fe_i-B_{Si} pairs. Their results are listed in Table V and compared with our calculated results. Here we see that the trends are reproduced quite nicely: As the distance to the acceptor is increased the energy of all localized gap states is lowered, which leads to the lowering of the electron removal energies as well. We note that for the Fe_i-B_{Si} pairs our total-energy results should be more accurate, primarily because there are no filled acceptor *d* shells.

Also included in Fig. 7 are results for a trigonal Fe_i-P_{Si} pair. Such a pair has been observed[4] experimentally via the disappearance of the concentration of the EPR signal ascribed to the isolated Fe_i^0. Our calculations confirm that the pair is stable for *n*-type samples when it is in its negatively charged state and can be considered as Fe_i^{2-}-P_{Si}^{+}. The charge state of the interstitial iron component of the pair is rather unusual. The attractive potential of the P_{Si}^{+} is strong enough to allow for a doubly negative charged state of the interstitial iron, which thereby has a completely filled *d* shell. We find that the pair is diamagnetic and therefore is EPR inactive. We obtain an acceptor level and a donor level for this pair at $E_v+0.8$ eV and $E_v+0.6$ eV, respectively, which are at energies where the pair is no longer stable.

TABLE IV. Comparison of calculated and experimental electron removal energies for iron-acceptor pairs (in eV).

	Theor.		Expt.	
Pair	$E(+/0)$	$E(0/-)$	$E(+/0)$	$E(0/-)$
		trigonal pairs		
FeB	0.27	0.66	0.10[a]	0.865[b]
FeAl	0.14	0.62	0.20[c]	
FeGa	0.42	0.93	0.24[c]	
FeIn	0.08	1.00	0.27[d]	
FeTl	0.20	0.85		
		orthorhombic pairs		
FeB	0.21	0.58	0.03[c]	0.73[e]
FeAl	0.06	0.66	0.13[c]	
FeGa	0.20	0.71	0.17[c]	
FeIn	0.36	1.07	0.16[c]	

[a]Reference 31.
[b]Reference 13.
[c]Reference 5.
[d]Reference 6.
[e]Reference 32.

TABLE V. Comparison of calculated electron removal energies for different Fe-B pairs compared with experimental data (in eV).

Pair	$E(+/0)$	$E(0/-)$	Expt.[a]
$C_{3v}A$	0.27	0.66	0.88
C_{2v}	0.21	0.58	0.73
$C_{3v}B$	0.12	0.62	0.62
$C_{3v}C$		0.53	0.62
$C_{3v}D$		0.39	

[a]Reference 32.

If we compare our results with cluster calculations of Assali and Leite[16–19] we find a severe discrepancy. Assali and Leite conclude from their charge densities that the pair binding is predominantly covalent, whereas from our calculations we find essentially ionic bonding: We also find that upon pairing all defect-related states are more or less shifted in energy and change their character significantly. However, not all states are likewise sensitive. The t_2-derived bonding states are strongly mixed in contrast to the antibonding states and to the *e*-derived states. As shown in Tables I and II and also in Figs. 2(a) and 6(a), the total induced electron densities of the pairs do not differ much from that of a rigid superimposition of the densities of isolated iron and acceptors.

The bonding is definitely different from that of the Fe_i-Ag_{Si} and Fe_i-Au_{Si} pairs.[35] For these pairs we have found a covalent binding that also results in a charge redistribution leading to a low-spin ground state. For these pairs we further find pair binding energies that are above 1 eV (in agreement with experimental data[36]) and depend only slightly on the position of the Fermi energy. All these characteristics are different from that observed (and calculated) for the iron-acceptor pairs.

We plan to show in a forthcoming paper[20] that our calculated particle densities provide us with a firm basis for the computation of the hyperfine interactions of the different iron-acceptor pairs. Although the agreement of calculated hyperfine data with experimental data gives some support to the validity of our results, we note that hyperfine interactions arise from the magnetization densities, while for the pair binding the total particle density is the key quantity.

ACKNOWLEDGMENTS

The authors have benefited from many fruitful discussions with Professor J.-M. Spaeth, Dr. S. Martini, and Dr. S. Greulich-Weber. H.W. is grateful to the Deutsche Forschungsgemeinschaft for financial support.

[1] K. Graff, in *Metal Impurities in Silicon-Device Fabrication*, edited by H. K. V. Lotsch, Springer Series in Materials Science Vol. 24 (Springer, Heidelberg, 1995).
[2] K. Graff and H. Pieper, J. Electrochem. Soc. **128**, 669 (1981).
[3] L.C. Kimmerling, in *Defects in Semiconductors*, edited by J. Narajan and T.Y. Tan (Elsevier, New York, 1981), p. 85.
[4] H. Takahashi, M. Suezawa, and K. Sumino, Mater. Sci. Forum **143-147**, 1257 (1994).
[5] A. Chantre and D. Bois, Phys. Rev. B **31**, 7979 (1985).
[6] A. Chantre and L.C. Kimmerling, Mater. Sci. Forum **10-12**, 387 (1986).
[7] P. Emanuelsson, W. Gehlhoff, P. Ohmling, and H.G. Grimmeiss, in *Impurities, Defects and Diffusion in Semiconductors: Bulk and Layered Structures*, edited by D. J. Wolford, J. Bernhole, and E. E. Haller, MRS Symposia Proceedings No. 163 (Materials Research Society, Pittsburgh, 1990), p. 307.
[8] P. Emanuelsson, P. Omling, H.G. Grimmeiss, W. Gehlhoff, and K. Irmscher, *The Physics of Semiconductors*, edited by Ping Jiang and Hou-Zhi Zheng (World Scientific, Singapore, 1992), p. 1717.
[9] W. Gehlhoff, K.H. Segsa, and C. Meyer, Phys. Status Solidi B **105**, K91 (1981).
[10] W. Gehlhoff and K.H. Segsa, Phys. Status Solidi B **115**, 443 (1983).
[11] W. Gehlhoff, K. Irmscher, and J. Kreissl, in *New Developements in Semiconductor Physics*, edited by G.G. Ferenczi and F. Beleznoy, Lecture Notes in Physics Vol. 301 (Springer-Verlag, Heidelberg, 1987), p. 262.
[12] W. Gehlhoff, P. Emanuelsson, P. Omling, and H.G. Grimmeiss, Phys. Rev. B **41**, 8560 (1990).
[13] S. Ghatnekar-Nilsson, M. Kleverman, P. Emanuelsson, and H.G. Grimmeiss, Mater. Sci. Forum **143-147**, 171 (1994).
[14] S. Greulich-Weber, A. Görger, J.-M.Spaeth, and H. Overhof, Appl. Phys. A **53**, 147 (1991).
[15] K. Irmscher, T. Kind, and W. Gehlhoff, Phys. Rev. B **49**, 7964 (1994).
[16] L.V.C. Assali and J.R. Leite, Mater. Sci. Forum **10-12**, 55 (1986).
[17] L.V.C. Assali and J.R. Leite, Phys. Rev. B **36**, 1296 (1987).
[18] L.V.C. Assali and J.R. Leite, Mater. Sci. Forum **38-41**, 409 (1989).
[19] L.V.C. Assali and J.R. Leite, Mater. Sci. Forum **83-87**, 143 (1992).
[20] H. Weihrich and H. Overhof (unpublished).
[21] P. Hohenberg and W. Kohn, Phys. Rev. **136**, B864 (1964).
[22] W. Kohn and L.J. Sham, Phys. Rev. **140**, A1133 (1965).
[23] U. von Barth and L. Hedin, J. Phys. C **5**, 1629 (1972).
[24] D. Ceperley, Phys. Rev. B **18**, 3126 (1978).
[25] D.M. Ceperley and B.J. Alder, Phys. Rev. Lett. **45**, 566 (1980).
[26] O. Gunnarsson, O. Jepsen, and O.K. Andersen, Phys. Rev. B **27**, 7144 (1983).
[27] F. Beeler, O.K. Andersen, and M. Scheffler, Phys. Rev. Lett. **55**, 1498 (1985); Phys. Rev. B **41**, 1603 (1990).
[28] F. Beeler and M. Scheffler, Mater. Sci. Forum **38-41**, 257 (1989).
[29] H. Weihrich and H. Overhof, Phys. Rev. B **54**, 4680 (1996).
[30] C.O. Rodriguez, S. Brand, and M. Jaros, J. Phys. C **13**, L333 (1980).
[31] M. Suezawa and M. Sumino, in *Impurities, Defects and Diffusion in Semiconductors: Bulk and Layered* (Ref. 7), p. 233.
[32] H. Nakashima, T. Sadoh, and T. Tsurushima, Phys. Rev. B **49**, 16 983 (1994); Mater. Sci. Forum **143-147**, 1191 (1994).
[33] L.C. Kimmerling, M.T. Asom, J.L. Benton, P.J. Drevinski, and C.E. Caefer, Mater. Sci. Forum **38-41**, 141 (1989).
[34] S. Zhao, L.V.C. Assali, and L.C. Kimmerling, Mater. Sci. Forum **196-201**, 1333 (1995).
[35] H. Overhof and H. Weihrich, Mater. Sci. Forum **196-201**, 1357 (1995).
[36] S.D. Brotherton, P. Bradley, and A. Gill, J. Appl. Phys. **57**, 1783 (1985).